REPORT DOCUMENTATION PAGE

Form Approved
OMB No. 0704-0188

PLEASE DO NOT RETURN YOUR FORM TO THE ABOVE ADDRESS.

1. REPORT DATE *(DD-MM-YYYY)*	2. REPORT TYPE	3. DATES COVERED *(From - To)*
05-12-2008	Final	27 09 2006-26 09 2008

4. TITLE AND SUBTITLE

Carbon Nanotube Array for Infrared Detection

5a. CONTRACT NUMBER

5b. GRANT NUMBER

W911NF-06-1-0480

5c. PROGRAM ELEMENT NUMBER

6. AUTHOR(S)

Xu, Jimmy

5d. PROJECT NUMBER

5e. TASK NUMBER

5f. WORK UNIT NUMBER

7. PERFORMING ORGANIZATION NAME(S) AND ADDRESS(ES)

Brown University
Division of Engineering
Box D, 184 Hope Street
Providence, RI 02912

8. PERFORMING ORGANIZATION REPORT NUMBER

9. SPONSORING/MONITORING AGENCY NAME(S) AND ADDRESS(ES)

US ARMY RDECOM ACQ CTR - W911NF
4300 S. Miami BLVD
Durham, NC 27703

10. SPONSOR/MONITOR'S ACRONYM(S)

11. SPONSOR/MONITOR'S REPORT NUMBER(S)

12. DISTRIBUTION/AVAILABILITY STATEMENT

Approved for Public Release, Distribution is unlimited

13. SUPPLEMENTARY NOTES

14. ABSTRACT

We explore the basic science issues and device potential of our carbon nanotube-silicon (CNT-Si) heretorjunctions for infrared photodetection. We focus on the underlying mechanism of infrared photocurrent response, which is elucidated by a detailed study of the dependence of the photocurrent on modulation frequency and intensity of the incident infrared radiation. The photocurrent generation is ascribed to the formation of the CNT-Si heterojunction, rather than the thermal gradient in the structure. The potential detectivity of the CNT photodiode is evaluated by considering the Auger recombination rate limit and found to be several thousand times greater than HgCdTe. The infrared photo-detection capability of the CNT-Si heterojunction is demonstrated by a comparison between the experimental photo-responses from Si and the carbon nanotubes. With the help of analytical formulas and simulation tools, we also investigate the temperature dependence of the 1D-3D heterodimensional CNT-Si heterojunction. These findings establish a basic understanding of this unique hetero-dimensional junction system and will help guide further development, design, and optimization.

15. SUBJECT TERMS

Carbon Nanotube, Silicon, Heterojunction, IR Detector.

16. SECURITY CLASSIFICATION OF:			17. LIMITATION OF ABSTRACT	18. NUMBER OF PAGES	19a. NAME OF RESPONSIBLE PERSON
a. REPORT	b. ABSTRACT	c. THIS PAGE			Xu, Jimmy
U	U	U	UU	16	19b. TELEPHONE NUMBER *(Include area code)* 401-863-1418

Reset

Carbon Nanotube Array for Infrared Detection

Final Report

Jimmy Xu
Division of Engineering, Box D
Brown University
Providence, RI 02912
401-863-1439
Jimmy_Xu@Brown.edu

Project start date 9/27/2006
ARO Proposal Number: 50493-EL
Agreement Number W911NF-06-1-0480
Managed by: Dr. Bill Clark, ARO Electronics Division Chief

Abstract

We explore the basic science issues and device potential of our carbon nanotube-silicon (CNT-Si) heretorjunctions for infrared photodetection. We focus on the underlying mechanism of infrared photocurrent response, which is elucidated by a detailed study of the dependence of the photocurrent on modulation frequency and intensity of the incident infrared radiation. The photocurrent generation is ascribed to the formation of the CNT-Si heterojunction, rather than the thermal gradient in the structure. The potential detectivity of the CNT photodiode is evaluated by considering the Auger recombination rate limit and found to be several thousand times greater than HgCdTe. The infrared photo-detection capability of the CNT-Si heterojunction is demonstrated by a comparison between the experimental photo-responses from Si and the carbon nanotubes. With the help of analytical formulas and simulation tools, we also investigate the temperature dependence of the 1D-3D heterodimensional CNT-Si heterojunction. These findings establish a basic understanding of this unique hetero-dimensional junction system and will help guide further development, design, and optimization.

NOTE: As of November 2008 the remaining options for this grant will not be exercised and our sponsored programs office will initiate the grant closeout procedures.

Table of contents

List of publications	4
Introduction	5
The underlying mechanism of photocurrent generation	5
Intensity dependence of the photo-response	7
Mechanism of photocurrent generation	8
Simulation results of nano-contact array	9
The reverse rectification of CNT-Si heterojunctions	10
Reaching beyond the original goal – establishing the feasibility of developing rectifying arrayed nano-scale antennas in the optical regime	11
Summary	15
References	16

List of Publications

Some of our findings and results have been reported in published or submitted papers to refereed journals as well as invited and contributed conference presentations.

Year 2 Publications:

1. T. F. Kuo, M. B. Tzolov, D. A. Straus and J. M. Xu. Electron transport characteristics of the carbon nanotubes/Si heterodimensional heterostructure." Applied Physics Letters 92 212107 (2008). Selected in June 9, 2008 issue of Virtual Journal of Nanoscale Science & Technology
2. T. F. Kuo, M. B. Tzolov, D. A. Straus and J. M. Xu. Infrared Detection and Electron Transport Characteristics of a Carbon nanotubes/Si Heterodimensional Heterostructure." Materials Research Society, Spring meeting (2008).
3. T. F. Kuo, D. A. Straus, M. B. Tzolov and J. M. Xu, "Electron transport in carbon nanotubes-silicon hetero-dimensional heterojunction: An experimental investigation", submitted to Physical Review B, in revision.
4. T. F. Kuo, M. B. Tzolov, D. A. Straus and J. M. Xu. Carbon Nanotube - Silicon heterojunction photocurrent response," in preparation.

Year 1 Publications:

1. M. B. Tzolov, T. F. Kuo, D. A. Straus, A. Yin and J. M. Xu, "Carbon nanotube-silicon heterojunction arrays and infrared photocurrent responses", Journal of Physical Chemistry C, **111** 5800 (2007).
2. D. A. Straus, M. B. Tzolov, T. F. Kuo, A. Yin and J. M. Xu, "Photocurrent response of the carbon nanotube–silicon heterojunction array" IET Circuits, Devices & Systems, **1**, 204, (2007).
3. D. A. Straus, M. B. Tzolov, T. F. Kuo, A. Yin, D. A. Cardimona and J. M. Xu ,"The carbon nanotube-silicon heterojunction as infrared detector", SPIE Photonics for Space Environments XI, **6308** 63080Q (2006).
4. T. F. Kuo, D. A. Straus, M. B. Tzolov and J. M. Xu, (invited) "Carbon Nanotube - Silicon Heterojunction Hyperspectral Photocurrent Response", Mater. Res. Soc. Symp. Proc., **963** 0963-Q22-01, (2007).
5. J. M. Xu, M. B. Tzolov, T. F. Kuo and D. A. Straus, (invited) "Arrayed carbon nanotube – silicon heterojunction: a new IV-IV semiconductor system and uncooled IR sensing", 2007 Workshop on Compound Semiconductors and ICs, Venice, Italy, May 20-23, 2007.

Introduction

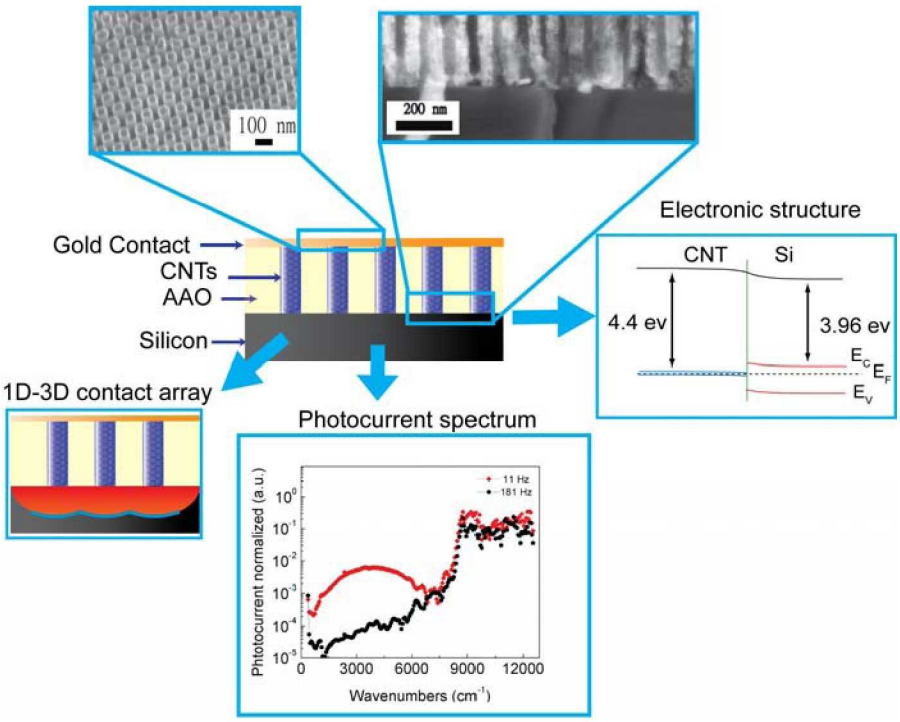

Fig.1 Some of the aspects of the carbon nanotube-Si heterojunction studied in this phase of development include: the temperature dependence of the CNT-Si heterodimentsional heterojunction contacts, the temporal characteristics of the photocurrent generation mechanism, the reverse rectification behavior of the CNT-Si heterojunction at small currents, and the intensity dependence of the photoresponse

As reported previously, we have successfully demonstrated the first controlled fabrication of a carbon nanotube-silicon (CNT-Si) heterostructure, and measured this structure's photocurrent response in the range from visible to mid-IR. Although smaller than the silicon response, the infrared response of the CNT-Si heterojunction is pronounced at room temperature. This represents the first clear evidence of infrared photocurrent response from a CNT-Si heterojunction system. The I-V curve indicates that SCL conduction with deep traps dominates the forward bias transport properties, which is also likely the reason for the slow photoresponse and is expected at the early stage of any new semiconductor device development. The measurements also reveal a temperature dependent change in current-voltage dependence from the 3/2-power law of a point-contact to the quadratic power law of a planar contact. We also observed that, in the reverse bias direction, the 1-D to 3-D dimensionality change at the heterojunction produced an enhanced tunneling to such an extent that a reverse rectifying effect results at low biases. In this phase of development, we studied the mechanism of photocurrent generation and provided a more detailed understanding of the hetero-dimensional heterostructure formed by carbon nanotubes and Si.

The underlying mechanism of photocurrent generation

The photocurrents in our device are clearly separated in the spectra because of the large difference in the absorption ranges of CNT's and Si. We used this spectral separation to find out if the time responses of the two components are different. The top time trace of the photocurrent signal in Fig. 2 was measured from turning on and off the broadband illumination (provided by the globar of the Bruker FTIR). The lower trace in the figure was taken using the same light source but containing light only below 4000 cm^{-1}, filtered out by a long pass filter. We observe the presence of two different time components in the top trace of the

photoresponse: a strong, very quickly rising photoresponse superimposed over a slower (in the range of a second) photoresponse of lower intensity. The lower time trace consists only of a component in the range of a second, matching the slow component in the top time trace. This simple comparison indicates that the fast component is solely due to absorption of higher energy photons. From this data, we hypothesize that the fast response originates from the silicon and the slower component from the carbon nanotubes.

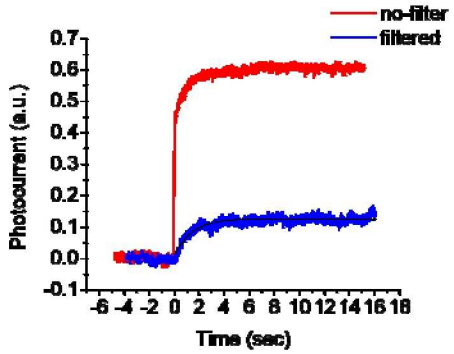

Fig.2 Time trace of the photocurrent when opening the shutter. Black curve in the figure shows the result of fitting with time constant of 0.8 seconds. The filter employed for the blue time-trace was a long pass 4000 cm^{-1} filter, which has the sole effect of cutting off the higher-speed silicon bandgap contribution.

After completing the spectral investigation of the sample's photocurrent, it became clear that the infrared response was characteristically slow; photocurrent spectroscopy was then repeated at phase modulation as slow as 5 Hz. The spectral shape of the mid-infrared band does not change at higher modulation frequencies; just the intensity decreases. This can be seen in Fig. 3. To precisely determine the time response of the CNT-Si heterojunction, FTIR photocurrent spectra were gathered at different modulation frequencies. This is a time consuming procedure, but once done it gives the frequency dependence of the signal with very good spectral discrimination, and from it the time constant can be estimated. The magnitudes of the peaks (both silicon and infrared) versus the mirror's modulation frequency are plotted in Fig. 4. The measurements were performed at room temperature and in the air. We can clearly see that the responses from Si and CNTs have quite different characteristic times.

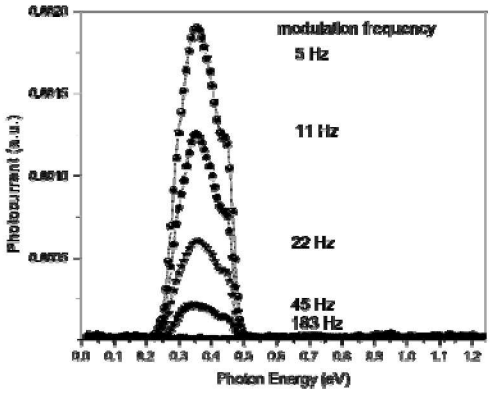

Fig.3 Infrared response of nanotubes at different modulation frequencies.

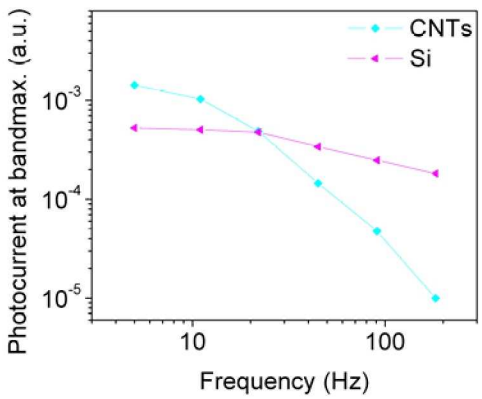

Fig.4 Double logarithmic plot of the frequency dependence of the bandmax amplitude for the silicon (diamonds) and for the carbon nanotubes (triangles) photoresponse.

Up to the highest frequency used, there is no significant change in the value for Si band, indicating that the time constant is less than 5 milliseconds. However, this is not the case for the longer wavelength CNTs response; it starts dropping very fast above a modulation of 10 Hz, which means the time constant is on the order of hundreds of milliseconds. This conclusion, based on the more precise data in Fig.4, corroborates the hypothesis for the slower time response of the infrared photocurrent generated in the carbon nanotubes.

Intensity dependence of the photo-response

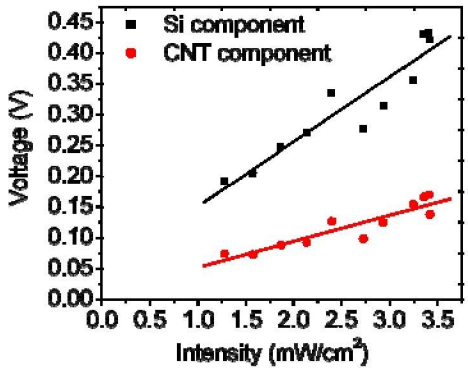

Fig.5 The amplitude of photocurrent vs. power of incident light.

In order to understand the relaxation process, we measured the dependence of the photocurrent on the incident light power. By varying the incident light intensity on the device, the amplitude of the photocurrent was recorded in the Fig. 5, which shows a linear relation for both Si and CNTs components. From a simple kinetic relation, if a bimolecular annihilation process were dominant, the rate of charge generation would depend on the square of the incident power, which is not the case for our structure. Instead, the linear relation between incident power and photocurrent suggests that decay of photocurrents are generated from the interactions of the photocarrier with impurity sites or traps, because the lifetime of carriers is determined by the number of traps or recombination centers, rather than photogenerated electron-hole pairs. At this limit, the on/off behavior of the photocurrent can be described by an exponential function $\Delta n = A(1 - \exp(-t / \tau))$. As shown in Fig. 2, the time constant extracted from the plot is 0.8 second, which matches the result from the photocurrent spectrum at different modulation frequencies. The result in Fig. 5 also reveals that the responsivity of the CNTs component is about 5 times smaller than the one from Si indicating that the performance figures of merit are not expected to be anywhere near their ultimate limits.

However, because the photo-carriers generated in Si and CNTs share the same conduction path, it is safe to assume that the same mechanism, like traps and interface states, reduces the photocurrent for both CNTs and Si. Note that this is at room temperature. In terms of absolute value, by taking into account the intensity of the illumination source, factoring in the amplification factor of the preamplifier, the area of the electrode contact, and the semi-transparency of the gold electrode, we get a value of the order of several tens of μA per watt. This result is both indicative of the potential and the need for further development and investigations. We suspect that many of the technology issues that are limiting the performance are rather similar to those in the early development of devices based on compound semiconductors. What is unique to carbon nanotubes, and might have played a role in our result, is the existence of metallic nanotubes. If present in the array, they would have provided a shunt path in addition to reverse leakage current. However, metallic nanotubes are more of an issue for ensembles of single-walled nanotubes, where the chirality is a critical parameter and very difficult to control.

Mechanism of photocurrent generation

The results presented in the previous section, however, naturally raise the question about the origin of the slower CNT response, since their carrier annihilation and recombination processes are normally quite fast, with a time constant shorter than tens of microseconds[1]. There are several possibilities. One possible explanation for the slow CNT response is the heating of CNTs upon light incidence. The thermal properties of carbon nanotubes are an interesting topic of research as CNT's might lend themselves to implementation in thermopile detectors or coatings in pyroelectric detectors. The presence of the highly absorptive arrayed nanotube film on silicon may play a role in establishing an efficient thermal gradient across the thickness of the silicon substrate contributing, albeit in a minor way, to the observed photocurrent response. In fact, the effect can be estimated by the experimental parameters. The broadband illumination from the globar source in the sample chamber of the Fourier spectrometer was estimated to be under 0.13 W/cm^2. The thermal conductivities of CNTs or carbon fibers and Si are about the same order[2], which is hundreds of Wm^{-1}K^{-1} and the thickness of the sample is about 500 μm including the silicon substrate and the CNT array. According to these parameters and the space-filling factor of the CNTs/AAO structure, the expected temperature difference between top and bottom of the device is about 10^{-6} K, which is almost negligible.

Nevertheless, although the temperature gradient can be small, the IR radiation can heat up the whole sample and higher temperature can assist the thermionic current thought the barrier. Again, one can estimate the characteristic time for heat dissipation, which can be described as the ratio between thermal capacitance (C) and conductance (G), i.e., ~ C/G. Because the thermal conductivity and specific heat of all of the materials in our structure are within the same order of magnitude, we can simply calculate the thermal time constant for a piece of sample with similar dimensions, which is 1×1×0.05 cm^3 in our experiments. Its specific heat capacity of 500 J/KgK and density of 2 g/cm^3 implies a calculated thermal time constant on the order of 20 milliseconds, which disagrees with our findings, i.e., the response due to thermal gradient should be significantly faster than observed infrared response. Therefore, it is reasonable to conclude that the mechanism of the infrared photoresponse is not thermal in origin.

The achievement of a non-thermal photoresponse from carbon nanotubes can be made even more encouraging by theoretically estimating their ultimate detection performance. The detectivity of an optimized infrared photo-detector can be generally expressed as $D \propto (\alpha/G)^{1/2}$, where α is the absorption coefficient and G is the thermal generation rate of carriers[3]. The absorption coefficient of CNTs in the 3 μm range can be as high as 3×10^4 cm^{-1}[4], compared to 1500 cm^{-1} for HgCdTe[3] . The ultimate performance of IR materials is also related to the thermal generation rate, which mostly depends on the Auger [5]. We assume that the Auger processes of in-template, CVD-grown CNTs is similar those of quantum well structures, because of the larger diameter of the CNTs in our experiments. As such, the carriers are confined to the walls of the CNTs. In quantum wells, the Auger rate for simple parabolic bands (also a valid approximation for CNTs' band structure) is found to be $R \propto \exp(-(2\mu+1/\mu+1)E_g / k_bT$ [6], where E_g is the bandgap, k_b is the Boltzmann constant and μ is the ratio of effective mass for electrons and heavy holes (m_c/m_v). Simple $k\cdot p$ theory shows that a small μ is naturally connected with a small gap[7]. The small ratio between electrons and holes makes the activation energy of the Auger process smaller and leads to a larger thermal generation rate. Because of the electron-hole symmetry in CNTs, the ratio of the

effective mass of electron and holes is close to unity. For comparison, the μ for HgCdTe is about 0.036 at room temperature[8]. This factor makes the exponent factor of the Auger rate of CNTs thousands of times smaller than of HgCdTe in the 3 μm detection range (400 meV). This can be even more pronounced at shorter wavelengths. Such an estimation of the ultimate performance of CNTs confirms their potential as infrared detection materials.

Simulation results of nano-contact array

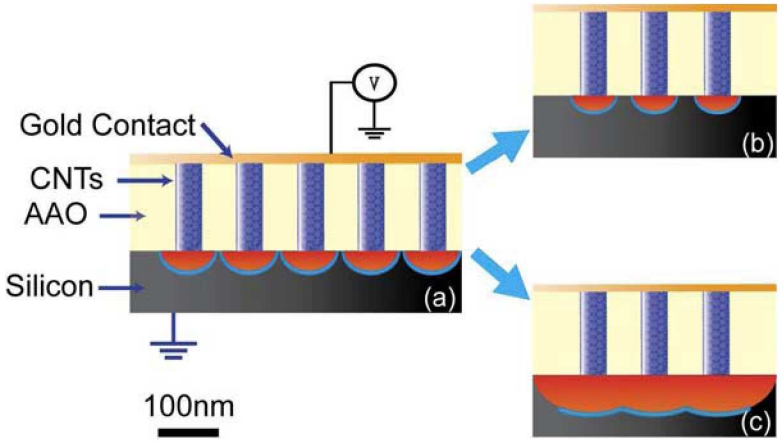

Fig. 6 Schematic of the nanotube-silicon heterojunction device structure, also illustrating the nature of the interface at 77K (a), 300K (b) and lower temperature(c). The doping of n-type Si substrate with 500μm thickness is 5 $\times 10^{15} cm^{-3}$. The lateral direction of the figure was drawn to the scale.

We have pointed out in our previous report that the transition between an array of nano-contacts and a planar contact can be attributed to the regular and small spacing of CNTs in the array, which is comparable to the screening range of the point contact at room temperature and becomes smaller than the growing screening range with decreasing temperature. To further validate the analysis, we performed a series of simulations in collaboration with Padre[9]. We used 24 nm as the radius of the carbon nanotubes and AAO as the surrounding material, both on top of a silicon substrate. The result is illustrated in Fig. 6, in which the blue regions depict the 1/e fall off distance (x_e) of the total potential drop in the conduction band. x_e is seen to be approximately 45nm for 300K (Fig. 6b) and larger than 50nm for 77K (Fig. 6a). The blue areas show the extent of the non-equilibrium electrical potential, characterized by a material related parameter, the Debye length. Because the Debye screening length in the silicon is shorter at 300K (Fig. 6b), the array of nanotubes acts as a collection of point-contacts. At lower temperatures (i.e. 77K (Fig. 6a)), the point contacts begin to merge into one another until they form a single planar junction (Fig. 6c). These results imply that the nature of the contact changes with respect to temperature, giving rise to the difference in SCL transport. The variation of the carrier concentration is more pronounced, since it is proportional to $\exp((E_f - E_c)/k_b T)$. We can see clearly from Fig.7 that at 77K, the fully depleted region extends over a 150nm range, while the center-to-center distance between carbon nanotube is about 110nm. This result again indicates that, the array of CNTs behave like a large electrode at 77K. On the other hand, the fully depleted region for 300K is much smaller than its counterpart at 77K and we may treat those nanotubes as individual contacts.

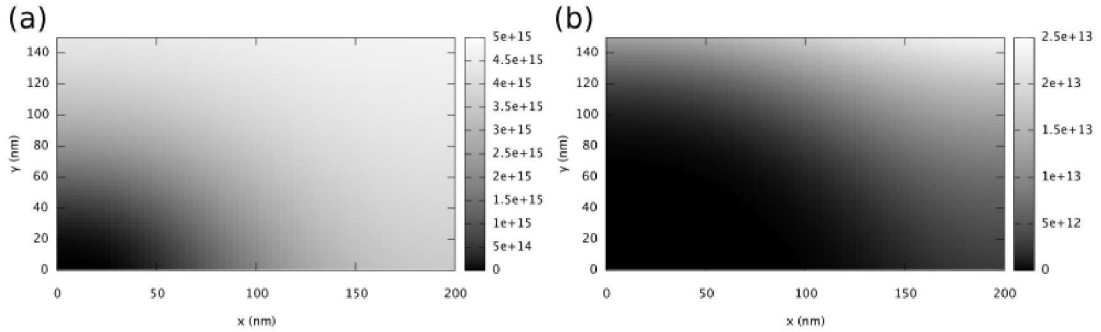

Fig. 7 The distribution of electron concentration (cm^{-3}) for the CNTs/Si heterojunction at 300K(a) and 77K(b). x and y are the distance from the long symmetrical axis of CNTs and the interface between CNTs and Si, respectively.

The reverse rectification of CNT-Si heterojunctions.

We previously reported the reversed rectification of the CNT-Si heterojunction. This time we performed a series of I-V measurements at different temperatures to gather more information on the reverse rectification. The inset of Fig. 8 shows the crossover voltage (i.e. the voltage at which the forward current becomes higher than the reverse current) at different temperatures. As expected, the crossover voltage increases with cooling because the relative contribution from either tunneling or field emission is greater at a lower temperature. When the temperature is high enough, the thermal (diffusion) current over the barrier in the forward direction would always dominate. More quantitatively, from the relation between the crossover voltage and temperature, one can extract the information of the barrier height and the related doping levels of the heterojunction. Because the bandgap of a CNT with large radius (~24 nm) is small, (~ 0.1 eV)[10] and because its conductivity is much higher than Si, one may model the CNT-Si heterojunction as a Schottky contact. The relation for forward diffusion current, in the presence of recombination centers or trap levels, can be written as[11],

$$j_f \cong j_s[\exp(\frac{qV_a}{2k_bT}) - 1],$$

While the tunneling current can be expressed as[12]

$$j_r \cong -j_s \exp(\beta\frac{-qV_a}{k_bT})[\exp(\frac{-qV_a}{k_bT}) - 1]$$

where j_s is saturation current density, V_a is the absolute value of the applied bias voltage, and T and k are temperature and Boltzmann constant, respectively. β is a dimensionless temperature dependent factor, which is defined as $\beta = 1 - T/T_1$ [12] and $T_1 = 2(\phi_b - V_a - \xi)^{1/2}/\kappa lk \equiv 2V^{1/2}/\kappa lk$, where $\kappa^2 = 2m^*/\hbar$, $l = (2\varepsilon_s\phi_b/qN_b)^{1/2}$. ξ is the energy of the conduction band with respect to the Fermi level, ε_s is the dielectric constant, ϕ_b is the barrier height and N_d is the doping of the semiconductor substrate. The condition that is necessary for reverse current to exceed forward current can be obtained from these equations: the dimensionless factor β has to be larger than *1/2 (β > 1/2)*. Therefore, the condition for "reverse" rectification can be obtained as

$$V^{1/2} > \frac{\phi_b^{1/2}k_bT}{E_{00}},$$

where E_{00} is an important parameter in tunneling and is defined as

$$E_{00} \equiv \frac{\hbar q}{2}\sqrt{\frac{N_d}{m^* \varepsilon_s}}\,.$$

Whether the condition for reverse rectification will be met depends on the values for the doping concentration and barrier height. Using the results from our experiment we found the effective barrier height $\phi_b = 0.32$V and $E_{00} = 7.2 \times 10^{-3}$ eV from the inset of Fig. 8 by extrapolating to zero temperature. The effective barrier height is close to the value predicted by the Anderson model with an E_{00} corresponding to $N_d = 2\times10^{17}$ cm^{-3}. In a conventional tunneling situation, the value of E_{00} determines the voltage-regimes of different transport mechanisms[13]. Our result shows that $qE_{00}/kT \sim 0.3$ at room temperature, which indicates that, at room temperature, the transport mechanism is on the border between thermionic and field emission. This result points to the significance of tunneling transport in our structure. This result can be understood as involving mutually the electric field enhancement and the narrowed barrier width.

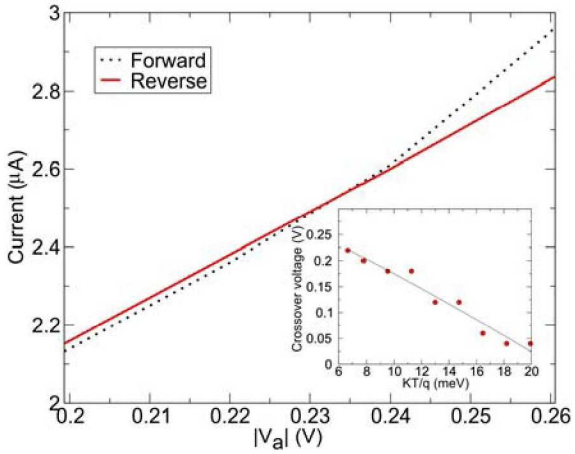

Fig. 8 Comparison of forward and reverse current at low bias at 77 K. This figure shows that reverse current is larger than forward current at lower voltage. The inset shows how crossover voltages change with temperatures. The solid line shows the best fit of the experimental results.

Reaching beyond the original goal – establishing the feasibility of developing rectifying arrayed nano-scale antennas in the optical regime

In the last months of this project, we have reached beyond the original goal and investigated the feasibility of developing a rectifying arrayed nano-scale antennas, in response to a formal request from Dr. Richard Osgood, Army Natick Center ARL. We have done preliminary feasibility studies and have obtained positive results on samples consisting of ordered arrays of vertically standing metal nano-antennas on silicon. The ordered array of nanoantennas is formed by depositing the metal through the AAO template onto an n-doped silicon substrate. The AAO is formed on the silicon substrate by the method described above. An SEM image of the resulting structure is shown in Fig. 9.

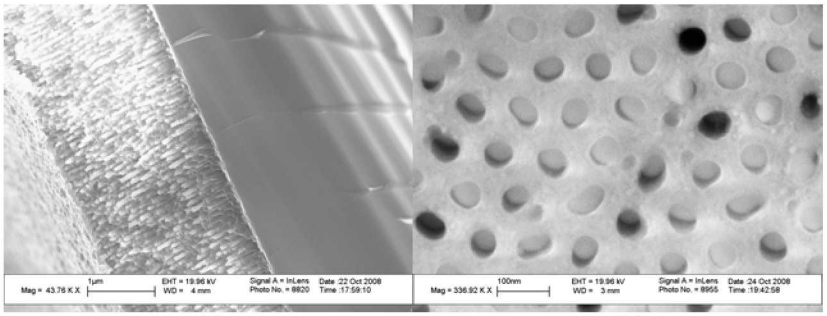

(a) **(b)**

Fig. 9 Gold nanoantennas formed by electro-less deposition of gold through the AAO template onto an n-type silicon substrate. The nanoantennas shown have a length of approximately 800nm and a diameter of approximately 40nm. (a) image is taken from a cleaved side of the sample. The antennas appear broken due to the imperfect cleaving of the AAO. (b) image taken from the top of the sample after top gold layer was removed showing gold-filled AAO pores.

The Schottky barrier that results from both the metal nanowire-silicon interface and the quasi-1D to 3D junction is expected to rectify the nanoantenna response, thus forming a rectenna. The response is also expected to depend on the nanoantenna parameters, such as the metal used in the nanoantenna fabrication, as well as the diameter and length of the nanoantenna. Previous theoretical studies of single metal nanoantennas [14] predict that the wavelength dependence of the nanoantenna response exhibits resonances at multiples of $\lambda_{eff} = n_1 + n_2\lambda/\lambda_p$, where λ_p is the plasma wavelength and n_1, n_2 are coefficients that depend on the material and geometry of the nanoantennas.

In this first stage of the project, we have established a method for the nanoantenna growth via the electro-less deposition of gold through the AAO template on an n-type silicon substrate. We are currently investigating a method for the electro-deposition of metals through the AAO that is expected to yield high quality nanoantennas, as well as more flexibility in terms of the metals from which the nanoantennas are made. The electro-deposition method we are currently investigating was previously studied by our group in the context of the electro-deposition of metals through the AAO on metallic substrates [15]. Our goal is to adapt and optimize that method for the case of a silicon substrate.

Also in this first stage of the project we have performed preliminary measurements for characterizing the optical and electrical properties of the nanoantenna assembly.

For the optical characterization, we have performed optical transmission and reflection measurements in the near infrared (NIR) and mid infrared (MIR) wavelength ranges. Figure 10 shows the NIR transmission and reflection of the sample after removal of the top gold contact layer. The series of peaks and valleys in the reflection spectrum is caused by the film interference generated by the AAO-Au matrix. Because of the presence of the embedded gold nanoantennas, the refractive index n of the AAO is increased. An approximate value for n can be extracted by fitting the inter-peak distances in Fig. 10 (a) to the formula $2dn = m\lambda$, where d is the AAO thickness, n is the refractive index, λ is the wavelength, and m is an integer. The value for n extracted by this procedure is approximately 5.3, disregarding the wavelength dependence.

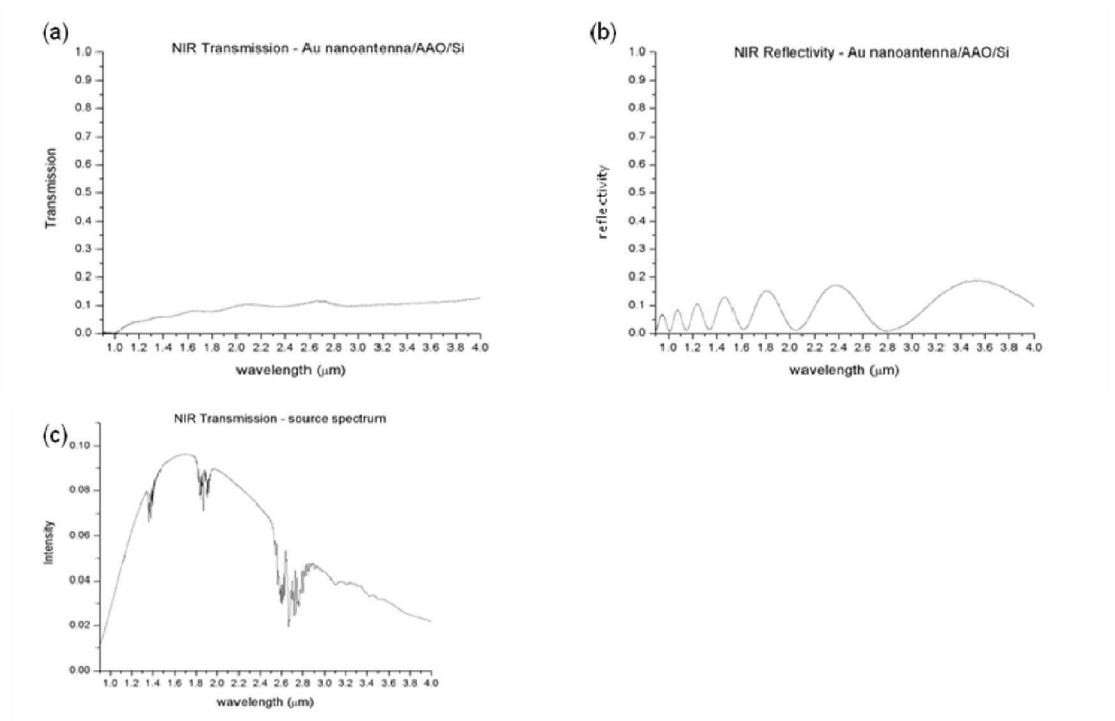

Fig. 10 (a) Near infrared transmission spectrum for a 800nm thick AAO film with gold nanoantennas on n-type silicon substrate. (b) Reflection spectrum. The peaks and valleys are caused by film interference effects from the AAO/nanoantenna assembly. (c) NIR source spectrum.

Figure 11 shows the transmission and reflection spectra for the MIR range. Resonances were found at 9μm in the transmission spectrum, and at 7.5μm and 8.5μm in the reflectivity spectrum. In order to further understand the origin of these resonances, additional measurements were made for an ordered assembly of gold nanoparticles (Fig. 12) created by evaporating gold on an n-type silicon substrate trough an AAO template mask and then removing the mask. The nanoparticle assembly transmission and reflection spectra showed similar resonances without the backgrounds of peaks and valleys caused by the AAO in the nanoantenna spectra.

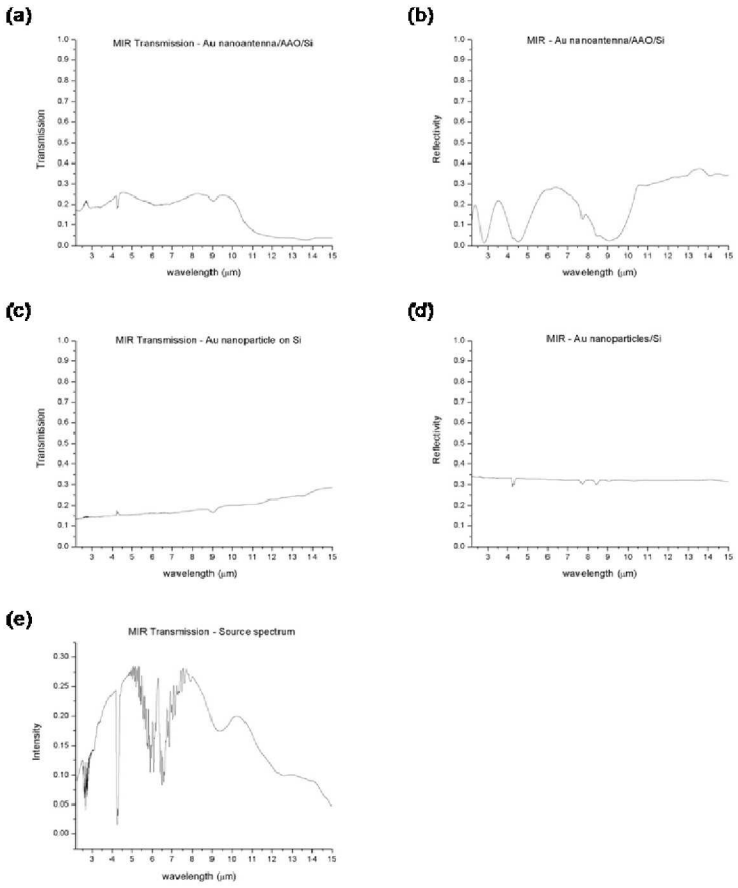

Fig. 11 (a) and (b) – MIR transmission and reflection spectra for gold nanoantenna array. (c) and (d) MIR transmission and reflection spectra for ordered assembly of gold nanoparticles on a silicon substrate (see Fig. 12). (e) MIR source spectrum.

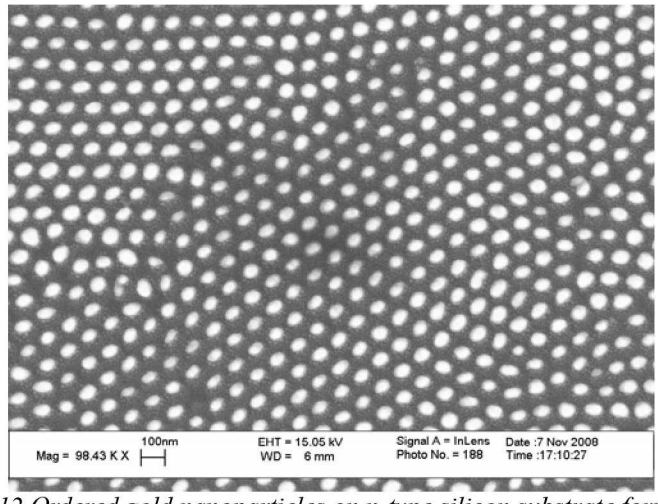

Fig. 12 Ordered gold nanoparticles on n-type silicon substrate formed by evaporating gold through an AAO mask.

In order to measure the I-V curve for the device, an appropriate ohmic contact must be evaporated on the back (silicon side) of the device. Aluminum was chosen as back contact because its work function (4.08eV) is within a few meV of the electron affinity of the silicon substrate (4.07eV). Figure 13 shows the sample I-V curve measured between the gold contact at the top of nanoantennas and the aluminum contact on the back side of the sample. The voltage is applied to the gold contact. The rectification exhibited indicates a Schottky contact between the gold nanoantennas and the silicon.

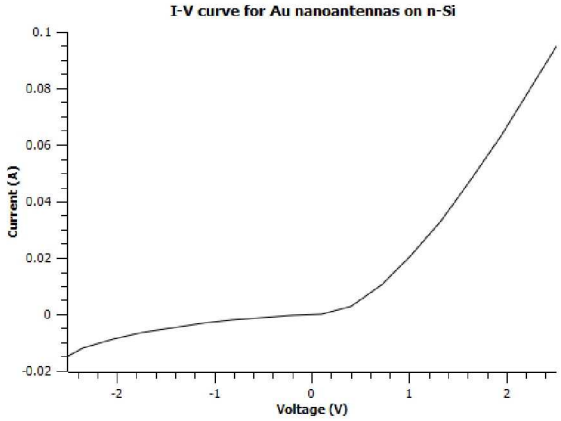

Fig. 13 I-V curve for the nanoantenna array sample with height of 800nm, diameter of 40nm and inter-antenna spacing of approximately 100nm.

In order to further investigate the optical properties of the nanoantenna array, we plan to measure reflectivity and absorption spectra in the visible range, as well as to measure the photocurrent response of the sample in the MIR, NIR, and Visible/UV wavelength ranges.

Summary

In this phase of development, we investigated the mechanism of photocurrent generation in the CNT-Si heterostructure by measuring the dependence between photo response and modulation frequencies and intensity of incident light. A calculation based on the estimated thermal properties of the device structure shows that the photocurrent due to heating is negligible, because the temperature gradient caused by optical absorption is too small. Furthermore, the characteristic time for heat dissipation disagrees with our experimentally measured infrared time response. The mechanism of the slow response in our structure, or of carbon nanotubes in general, is still under investigation. The coexistence of the silicon photocurrent response naturally extends the spectral range of the device to visible wavelengths; it is part of the intrinsic function of the heterojunction. The simulated data shows that the spatial extent of the depletion (effective contact) region under the nanotube tip shrinks with increasing temperature. The shrinking is more appreciable laterally, from > 50nm at 77K, in which case the individual arrayed contact regions effectively merge into one, to < 45nm at 300K, in which case the individual contact regions become spatially separated. The reverse current in the CNT-Si heterojunction, however, exhibits two distinctively different regimes – one is an unusual reverse rectification in the small bias regime, and the other is the normal rectification regime at larger biases. We attribute to the unusual reverse rectification behavior to the unique enhancement of the electric field due to the vertical standing nanotube forming a 1-D point contact to a 3-D bulk which in turn gives rise to an exponential increase in the tunneling. These unusual phenomena, while being interesting in terms of quantum transport in low-dimensional systems, might be exploited for applications requiring voltage-controlled nonlinearity. In terms of future research directions for the CNT-Si heterojunction system, we have started testing a pre-annealing and hydrofluoric acid treatment step in order to ensure complete removal of the SiO_2 residue layer at the bottom of the AAO pores prior to CNT growth. Additionally, we have introduced in our sample processing flowchart a post-processing reactive ion etch step to remove the top carbon layer that covers CNT-AAO matrix after CNT growth. These two modifications are expected to increase the photoresponse and improve the overall performance of our

devices. We are also currently investigating the effect of the CNT diameter (and hence band-gap energy), pore spacing, as well as CNT length on the photocurrent responsivity spectra of the CNT-Si heterojunction. Reaching beyond our originally proposed goal, we have started exploring the possible application of a system consisting of arrays of vertically standing metal nanoantennas on silicon substrate as a platform for detection of light in both the infrared and visible ranges, as detailed in the section above.

References

1. Batista, J., A. Mandelis, and D. Shaughnessy, *Temperature dependence of carrier mobility in Si wafers measured by infrared photocarrier radiometry.* Applied Physics Letters, 2003. **82**(23): p. 4077-4079.
2. Heremans, J., I. Rahim, and M.S. Dresselhaus, *Thermal-Conductivity and Raman-Spectra of Carbon-Fibers.* Physical Review B, 1985. **32**(10): p. 6742-6747.
3. Piotrowski, J. and W. Gawron, *Ultimate performance of infrared photodetectors and figure of merit of detector material.* Infrared Physics & Technology, 1997. **38**(2): p. 63-68.
4. Itkis, M.E., et al., *Bolometric Infrared Photoresponse of Suspended Single-Walled Carbon Nanotube Films*. 2006. p. 413-416.
5. Gerhardts, R.R., R. Dornhaus, and G. Nimtz, *Auger-Effect in Hg1-Xcdxte.* Solid-State Electronics, 1978. **21**(11-1): p. 1467-1470.
6. Smith, C., R.A. Abram, and M.G. Burt, *Auger Recombination in a Quantum Well Heterostructure.* Journal of Physics C-Solid State Physics, 1983. **16**(5): p. L171-L175.
7. Kittel, C., *Quantum theory of Solids*. 2 ed. 1987, New York: Wiley.
8. Rogalski, A., *HgCdTe infrared detector material: history, status and outlook.* Reports on Progress in Physics, 2005. **68**(10): p. 2267-2336.
9. Vasileska, D. and G. Klimeck, *Padre*. 2006.
10. Davydov, D.N., et al., *Resistance and tunneling spectra of aligned multiwalled carbon nanotube arrays.* Journal of Applied Physics, 2000. **88**(12): p. 7205-7208.
11. Chih-Tang, S., R.N. Noyce, and W. Shockley, *Carrier Generation and Recombination in P-N Junctions and P-N Junction Characteristics*. Proceedings of the IRE, 1957. **45**(9): p. 1228-1243.
12. Wilson, A.H., *A Note on the Theory of Rectification.* Proceedings of the Royal Society of London. Series A, Containing Papers of a Mathematical and Physical Character (1905-1934), 1932. **136**(830): p. 487-498.
13. Rhoderick, E.H. and R.H. Williams, *Metal-semiconductor contacts*. 1988, New York: Oxford University Press.
14. Novotny, L., *Effective Wavelength Scaling for Optical Antennas,* Phys. Rev. Lett., **98**, 266802, (2007).
15. Yin, A.J., Li, J., Jian, W., Bennett, A.J., Xu, J.M., *Fabrication of Highly Ordered Metallic Nanowire Arrays by Electrodeposition*, Appl. Phys. Lett., 79(7), 1039-1041, (2001).